

UC San Diego

UC San Diego Previously Published Works

Title

Prion protein post-translational modifications modulate heparan sulfate binding and limit aggregate size in prion disease.

Permalink

<https://escholarship.org/uc/item/07v1f58m>

Authors

Callender, Julia
Sevillano, Alejandro
Soldau, Katrin
et al.

Publication Date

2020-08-01

DOI

10.1016/j.nbd.2020.104955

Peer reviewed



Published in final edited form as:

Neurobiol Dis. 2020 August ; 142: 104955. doi:10.1016/j.nbd.2020.104955.

Prion protein post-translational modifications modulate heparan sulfate binding and limit aggregate size in prion disease

Julia A. Callender¹, Alejandro M. Sevillano^{1,^}, Katrin Soldau¹, Timothy D. Kurt^{1,^^}, Taylor Schumann¹, Donald P. Pizzo¹, Hermann Altmeppen², Markus Glatzel², Jeffrey D. Esko³, Christina J. Sigurdson^{1,4,#}

¹Departments of Pathology and Medicine, UC San Diego, La Jolla, CA 92093, USA

²Institute of Neuropathology, University Medical Center Hamburg-Eppendorf (UKE), Hamburg, Germany

³Department of Cellular and Molecular Medicine, UC San Diego, La Jolla, CA 92093, USA

⁴Department of Pathology, Immunology, and Microbiology, UC Davis, Davis, CA 95616, USA

Abstract

Many aggregation-prone proteins linked to neurodegenerative disease are post-translationally modified during their biogenesis. *In vivo* pathogenesis studies have suggested that the presence of post-translational modifications can shift the aggregate assembly pathway and profoundly alter the disease phenotype. In prion disease, the N-linked glycans and GPI-anchor on the prion protein (PrP) impair fibril assembly. However, the relevance of the two glycans to aggregate structure and disease progression remains unclear. Here we show that prion-infected knockin mice expressing an additional PrP glycan (tri-glycosylated PrP) develop new plaque-like deposits on neuronal cell membranes, along the subarachnoid space, and periventricularly, suggestive of high prion mobility and transit through the interstitial fluid. The plaque-like deposits were largely non-congophilic and composed of full length, uncleaved PrP, indicating retention of the glycoposphatidylinositol (GPI) anchor. Prion aggregates sedimented in low density fractions following ultracentrifugation, consistent with oligomers, and bound low levels of heparan sulfate similar to other predominantly GPI-anchored prions. These results suggest that highly glycosylated PrP primarily converts as a GPI-anchored glycoform with low involvement of HS co-factors, limiting PrP assembly mainly to oligomers. Thus, these findings may explain the high frequency of diffuse, synaptic, and plaque-like deposits and rapid conversion commonly observed in human and animal prion disease.

Corresponding author: Dr. Christina J. Sigurdson, Department of Pathology, UC San Diego, 9500 Gilman Dr., La Jolla, CA 92093-0612, USA. Phone: +1 (858) 534 0978, csigurdson@ucsd.edu.

[^]Current address: MD Anderson Cancer Center. 6767 Garnet Ave, Houston, TX

^{^^}Current address: Foundation for Food and Agriculture Research, 401 9th St NW, Ste. 630, Washington, DC 20001, USA.

Author contributions

JAC, AMS, TDK, and CJS conceived the study and designed the experiments, HA and MG provided reagents, JAC, AMS, KS, TDK, TS, and DPP performed the experiments, JAC, AMS, and JDE conducted the data analysis, and JAC and CJS wrote the manuscript, with input from AMS, HA, MG, and JDE.

Declaration of Competing Interest

The authors declare no competing financial interests.

Keywords

amyloid; neurodegeneration; glycosaminoglycans; ADAM10 cleavage; glycans; glycosylation; protein misfolding; prion strains

Introduction

Protein aggregation and neuronal loss are defining features of neurodegenerative disease [29, 32, 65], including prion disease [4]. In prion disease, the clinical progression is extraordinarily rapid, with a median survival of approximately six months for patients with sporadic Creutzfeldt-Jakob disease (sCJD) [28, 74, 75]. A causal role for the aggregated prion protein, PrP^{Sc}, in disease development has been established [46, 47], supported most recently by studies showing disease induction from recombinant PrP fibrils [10, 16, 69]. Compared to amyloid- β fibrils that display limited structural polymorphs [53], prion aggregates are remarkably diverse, forming a wide range of polymorphs [56] and appearing histologically as diffuse, punctate, plaque-like, or congophilic plaques that vary biochemically [8, 42]. Similar to other proteins that aggregate in neurodegenerative disorders, PrP is post-translationally modified [5, 19, 51, 60–62], yet how PrP post-translational modifications contribute to the aggregate conformation, co-factor interactions, and disease progression is unclear.

PrP^C is a ubiquitously expressed monomeric protein composed of 208 amino acids [13, 41] maintained in the outer plasma membrane by a glycosphosphatidylinositol (GPI)-anchor [5, 51]. The N-terminus is largely unstructured, whereas the C-terminal globular domain is composed of three α -helices with up to two N-linked glycans and a single disulfide bond that enhances protein stability [49]. During prion disease, PrP^C undergoes a major structural transformation from largely α -helical to β -sheet [6, 12]. PrP^{Sc} multimers template the misfolding of PrP^C, exponentially increasing PrP^{Sc} levels [52, 63].

Prion diseases are considered amyloid disorders, yet amyloid plaques composed of ultrastructurally visible fibrils are uncommon in sporadic human and animal prion disease [26, 74]. Notably, the prion protein is an atypical amyloidogenic protein, as it is relatively large, highly structured, glycosylated, and GPI-anchored. GPI-anchorless PrP aggregates assemble as fibrils in humans and in experimental models [14, 25, 31], suggesting that the GPI-anchor hinders fibril formation.

N-linked glycans may also limit PrP fibril formation. Glycans stabilize proteins [15, 20, 45], facilitate proper folding in the endoplasmic reticulum [66, 70] and may impair fibril formation by shielding and stabilizing intramolecular disulfide bonds, as shown for a human PrP glycopeptide (175–195) [7]. Glycans may also decrease PrP interactions with anionic co-factors and potential scaffolds for fibril formation, such as sulfated glycosaminoglycans [54]. However, glycans have been also shown to facilitate oligomer formation, depending on the chemical composition and location of the sugar present [38].

Thus on the one hand, glycans may stabilize the tertiary structure of PrP^C, raising the energy barrier for conversion and prolonging survival time. On the other hand, glycans may not

alter the barrier for conversion but only hinder fibril elongation, restricting prions to small oligomers that transit readily through the brain thereby accelerating disease progression. To better understand the impact of PrP glycans on prion disease, we previously inoculated *Prnp*^{187N} knockin mice, expressing PrP^C with up to three glycans, with a fibrillar plaque-forming strain known as mCWD [55]. Interestingly, the neuropathological phenotype switched from plaques to fine, granular PrP^{Sc} deposits, and the survival time dropped by 60% as compared to infected wild type (WT) mice [54]. Conversely, mice expressing unglycosylated PrP (*Prnp*^{180Q,196Q}) inoculated with two non-plaque-forming prion strains instead developed large plaques (approximately 100 μm) containing ADAM10-cleaved PrP^{Sc}, which suggests that glycans inhibit fibril formation. To help resolve the question of how PrP glycans on the carboxy terminus impact prion disease, here we inoculated *Prnp*^{187N} mice with four prion strains and determined survival times and prion distribution in the brain and spinal cord. We used an antibody targeting ADAM10-cleaved PrP [35] to measure the cleaved PrP^{Sc} levels, and mass spectrometry to measure the level and composition of prion-bound heparan sulfate (HS), which binds to plaque-forming prions [37, 54, 57, 59]. We found that all four prion strains were readily converted and showed a similar or slightly longer survival time than WT mice, yet with less spongiform change in the brain. Additionally, for two of four strains, mice developed plaque-like aggregates, which associate with neuronal membranes, retain the GPI-anchor, bind low levels of HS, and sediment in low density iodixanol fractions after ultracentrifugation, suggestive of smaller or less compact multimers. Finally, we compare our results to highly glycosylated human and animal prions, and propose a model for how glycans may underlie the extraordinary diversity in aggregate morphology and survival time in prion disease.

Materials and Methods

PrP^C expression in uninfected wild-type and *Prnp*^{187N} brain

To measure total PrP^C levels in WT (C57BL/6) and *Prnp*^{187N} brain samples, 40 μg of 10% brain homogenate from uninfected mice was lysed in 2% N-lauryl sarcosine. Samples were then incubated for 15 minutes at 37 °C shaking at 1000 rpm. NuPage loading dye (Invitrogen) was added and samples were heated at 95 °C for 6 minutes prior to electrophoresis and transfer to nitrocellulose. Membranes were incubated in either anti-PrP antibody POM1 (epitope in the globular domain, amino acids 121–231 of the mouse PrP) [43], A228 antibody against ADAM 10-cleaved PrP (sPrP^{G228} epitope at residue 228G [35]), or anti β-tubulin as a loading control (Cell Signaling Technology) and developed using chemiluminescent substrate. The chemiluminescent signals were captured and quantified using the Fuji LAS 4000 imager and Multigauge V3.0 software.

Structure Modeling

Images were created using PyMol version 2.3.3. PrP crystal structure was obtained from PDB ID code 1AG2. N-linked glycans were modeled using the Glycam glycoprotein builder [27]. Tetra-antennary, sialic acid-containing N-linked glycans were chosen for the purposes of modeling due to evidence that the pool of PrP N-linked glycans contain bi-, tri-, and tetra-antennary glycans that contain primarily 2,6-linked sialic acid [30, 50].

Prion transmission experiments in mice

Groups of 4–11 male and female *Prnp*^{187N} and WT (C57BL/6) mice were anesthetized with ketamine and xylazine and inoculated into the left parietal cortex with 30 µl of 1% prion-infected brain homogenate prepared from terminally ill mice. The prion strains used for inoculation were mouse-adapted RML, 22L, ME7, and mNS. The RML, 22L, and ME7 are cloned prion strains that have been maintained in C57BL/6 mice [3, 9, 17, 18], while mNS inoculum was derived from repeated passage of a single scrapie-infected sheep brain [3, 55] propagated in *tga20* and WT (C57BL/6) mice. For the serial passages of prions in *Prnp*^{187N} mice, homogenates from individual mouse brains were used. As negative controls, groups of age-matched WT (C57BL/6) and *Prnp*^{187N} mice (n= 4–5 mice/ group) were inoculated intracerebrally with mock brain homogenate from uninfected WT mice and housed under the same conditions as the prion-infected-mice.

Mice were maintained under specific pathogen-free conditions on a 12:12 light/dark cycle, and monitored three times weekly for the development of prion disease, including weight loss, ataxia, kyphosis, stiff tail, hind leg clasp, and hind leg paresis. Mice were euthanized at the onset of terminal clinical signs, and the incubation period was calculated from the day of inoculation to the day of terminal clinical disease. During the necropsy, one hemi-brain was formalin-fixed, then immersed in 96–98% formic acid for 1 hour, washed in water, and post-fixed in formalin for 2–4 days. Hemi-brains were then cut into 2 mm transverse sections and paraffin-embedded for histological analysis. The remaining brain sections were frozen for biochemical analyses.

Histopathology and immunohistochemical stains

Four micron sections were cut onto positively charged silanized glass slides and stained with hematoxylin and eosin (HE), or immunostained using antibodies for total PrP (SAF84) (Cayman Chemical), astrocytes (glial fibrillary acidic protein, GFAP), and heparan sulfate (10E4)(AMS Bioscience). PrP (SAF84; 1:400) and GFAP immunolabelling (DAKO; 1:6,000) was performed on an automated tissue immunostainer (Ventana Discovery Ultra, Ventana Medical Systems, Inc) with antigen retrieval performed by heating sections in a Tris-based EDTA buffer at 95 °C for 92 minutes or using a protease treatment (P2, Ventana) for 16 minutes, respectively. For HS immunolabelling, epitope retrieval was performed by placing sections in citrate buffer (pH 6), heating in a pressure cooker for 20 minutes, cooling for 5 minutes, and washing in distilled water. Sections were blocked and incubated with anti-heparan sulfate antibody for 45 minutes followed by anti-mouse biotin (Jackson Immunolabs; 1:250) for 30 minutes and then streptavidin-HRP (Jackson Immunoresearch) for 45 minutes. Slides were then incubated with DAB reagent (Thermo Scientific) for 15 minutes. Sections were counterstained with hematoxylin. Control slides for the HS stain were treated with heparin lyases I,II, III at 37 °C for 60 minutes prior to immunolabelling. To quantify plaque size in ME7 and mNS-infected mice, brain sections containing plaques were imaged at high magnification (400X) and the diameter at the largest point of the plaque was measured using ImageJ software (N = 35 plaques or plaque-like deposits from three mice per group).

For the Congo red staining, slides were deparaffinized, fixed in 70% ethanol for 10 minutes, immersed in an alkaline solution and then stained with Congo red solution overnight.

For the CD9 and total PrP co-immunostain of brains sections, epitope retrieval was first performed by immersing the sections in 96% formic acid for 5 minutes, digesting sections with 5 µg/ml PK for 10 minutes, and then heating slides in citrate buffer within a pressure cooker for 20 minutes, washing slides between each step. CD9 and PrP were labelled using anti-CD9 and anti-PrP antibodies (CD9: Novus; PrP: SAF84 from Cayman Chemical), and then sequentially, anti-rabbit HRP followed by tyramide-Alexa488 (CD9) followed by anti-mouse CY3, to label CD9 and PrP, respectively.

Lesion profile

Brain lesions from prion-infected WT (C57BL/6) and *Prnp*^{I87N} mice were scored for the level of spongiosis, gliosis, and PrP immunological reactivity on a scale of 0–3 (0= not detectable, 1= mild, 2= moderate, 3= severe) in 7 regions including grey and white matter: (1) dorsal medulla, (2) cerebellum, (3) hypothalamus, (4) medial thalamus, (5) hippocampus, (6) medial cerebral cortex dorsal to hippocampus, and (7) cerebral peduncle. A sum of the three scores resulted in the value obtained for the lesion profile for the individual animal and was depicted in the ‘radar plots’. Two investigators blinded to animal identification performed the histological analyses. Groups of 4–6 mice were analyzed for each strain.

PK-resistant PrP^{Sc} analyses

Brain homogenates were lysed in 2% N-lauryl sarcosine in PBS and incubated in PBS or digested with 50 µg/ml PK for 30 minutes at 37 °C prior to western blotting. Membranes were incubated with monoclonal antibody POM1, POM19 (epitope in the globular domain), POM2 (epitope in the flexible N-terminal tail), or POM3 (epitope in the flexible N-terminal tail) where indicated [43].

For measuring shed PrP^{Sc} by western blot, PrP^{Sc} from ME7- and mNS-infected *Prnp*^{I87N} mice and mCWD-infected mice was concentrated from 10% brain homogenate by performing sodium phosphotungstic acid precipitation prior to western blotting [68]. In brief, 10% brain homogenate in an equal volume of 4% sarkosyl in PBS was digested with benzonase™ (Sigma) followed by treatment with 100 µg/ml PK at 37 °C for 30 minutes. After addition of 4% sodium phosphotungstic acid in 170 mM MgCl₂ and protease inhibitors (Complete TM, Roche), extracts were incubated at 37 °C for 30 minutes and centrifuged at 18,000 *g* for 30 minutes at 25 °C. Pellets were resuspended in 2% N-lauryl sarcosine prior to electrophoresis and immunoblotting. Membranes were incubated with monoclonal antibody POM19 [43] or polyclonal antibody sPrP^{G228} [35] followed by incubation with an HRP-conjugated IgG secondary antibody. The blots were developed using a chemiluminescent substrate (Supersignal West Dura ECL, ThermoFisher Scientific) and visualized on a Fuji LAS 4000 imager. Quantification of PrP^{Sc} glycoforms and total PrP^{Sc} was performed using Multigauge V3 software (Fujifilm).

Velocity Sedimentation

Brain homogenate [10% in PBS (w/v)] from WT (C57BL/6) or *Prnp*^{187N} mice was lysed in velocity sedimentation lysis buffer (100 mM Tris-HCl pH 7.5, 150 mM NaCl, 1% N-lauryl sarcosine, final) for 30 minutes, carefully placed over a 4 – 24% step gradient (4%, 8%, 12%, 16%, 20%, and 24%), and centrifuged at 150,000 *g* for 1 hour. Fourteen fractions were collected from each tube, with the final fraction including the resuspended pellet. Aliquots of each fraction were digested with 50 µg/ml of PK for 30 min at 37 °C prior to immunoblotting and probing with anti-PrP antibody, POM19 [43].

Purification of PrP^{Sc} for mass spectrometry studies

PrP^{Sc} was purified from mouse brain following previously described procedures [48], with minor modifications. 10% brain homogenate was mixed with an equal volume of TEN(D) buffer [5% sarkosyl in 50 mM Tris-HCl, 5 mM EDTA, 665 mM NaCl, 0.2 mM dithiothreitol, pH 8.0), containing complete TM protease inhibitors (Roche)] and incubated on ice for 1 hour prior to centrifugation at 18,000 *g* for 30 minutes at 4 °C. All but 100 µl of supernatant was removed, and the pellet was resuspended in 100 µl of residual supernatant and diluted to 1 ml with 10% sarkosyl TEN(D). Each supernatant and pellet was incubated for 30 minutes on ice and then centrifuged at 22,000 *g* for 30 minutes at 4 °C. Supernatants were recovered while pellets were held on ice. Supernatants were added to ultracentrifuge tubes with 10% N-lauryl sarcosine TEN(D) buffer containing protease inhibitors and centrifuged at 150,000 *g* for 2.5 hours at 4 °C. Supernatants were discarded while pellets were rinsed with 100 µl of 10% NaCl in TEN(D) buffer with 1% sulfobetaine (SB3–14) and protease inhibitors and then combined with pellets and centrifuged at 225,000 *g* for 2 hours at 20 °C. The supernatant was discarded and pellet was washed and then resuspended in ice cold TMS buffer containing protease inhibitors (10 mM Tris-HCl, 5 mM MgCl₂, 100 mM NaCl, pH 7.0). Samples were incubated on ice overnight at 4 °C. Samples were then incubated with 25 units/ml benzonaseTM (Sigma-Aldrich) and 50 mM MgCl₂ for 30 minutes at 37 °C followed by a digestion with 10 µg/ml PK for 1 hr at 37 °C. PK digestion was stopped by incubating samples with 2 mM PMSF on ice for 15 minutes. Samples were incubated with 20 mM EDTA for 15 minutes at 37 °C. An equal volume of 20% NaCl was added to all tubes followed by an equal volume of 2% SB3–14 buffer. For the sucrose gradient, a layer of 0.5 M sucrose in buffer [100 mM NaCl, 10 mM Tris, and 0.5% SB3–14 (pH 7.4)] was added to ultracentrifuge tubes. Samples were then carefully overlaid on a sucrose layer and the tubes topped with TMS buffer. Samples were centrifuged at 200,000 *g* for 2 hours at 20 °C. The pellet was rinsed with 0.5% SB3–14 in PBS, resuspended in 50 µl of 0.5% SB3–14 in deionized water, and stored at –80 °C. Gel electrophoresis and silver staining were performed to assess the purity of brain extracts. To quantify PrP levels, samples were compared against a dilution series of recombinant PrP by immunoblotting and probing with the anti-PrP antibody POM19 [43].

Heparan sulfate purification and analysis by mass spectrometry

Heparan sulfate (HS) was extracted from the purified PrP^{Sc} preparation or from whole brain homogenate (10%, w/v) by anion exchange chromatography as described previously [1]. Purified PrP^{Sc} and brain homogenates were denatured in 0.5 M NaOH (final concentration)

on ice at 4 °C for 16 hours, neutralized with 0.5 M acetic acid (final concentration), and digested with pronase for 25 hours at 37 °C. HS was then purified by diethyl-aminoethyl (DEAE) sepharose chromatography (Healthcare Life Sciences), and digested with 1 milli-unit each of heparin lyases I, II, and III to depolymerize the HS chains. The disaccharides were then tagged by reductive amination with [¹²C₆]aniline [34] and mixed with [¹³C₆]aniline-tagged disaccharide standards. Samples were analyzed by liquid chromatography-mass spectrometry (LC-MS) using an LTQ Orbitrap Discovery electrospray ionization mass spectrometer (ThermoFisher Scientific). Internal disaccharides and nonreducing end monosaccharides were identified based on their unique mass and quantified relative to the HS weight [33, 34].

Statistics

A Student's *t* test (two-tailed, unpaired) was used to determine the statistical significance between the *Prnp*^{187N} versus WT mouse brain samples for the PrP^C level of expression, levels of ADAM10-cleaved PrP^C and PrP^{Sc}, as well as levels of HS bound to PrP^{Sc} in ME7-infected WT and *Prnp*^{187N} brains. One-way ANOVA with Tukey's post test was performed to assess survival differences between mouse groups. Two-way ANOVA with Bonferroni's post test was performed to assess differences in the lesion profiles, the glycoprofiles of PrP^{Sc} in WT and *Prnp*^{187N} mice infected with the four different PrP^{Sc} strains, and the composition of HS bound to PrP^{Sc} in ME7-infected *Prnp*^{187N} and WT mouse brain. GraphPad Prism 5® software was used for statistical analyses. No measurement was excluded for statistical analysis. For all analyses, *P* < 0.05 was considered significant. Data displayed in graphs represent mean ± SEM.

Study approval

All animal studies were performed following procedures to minimize suffering and were approved by the Institutional Animal Care and Use Committee at UC San Diego. Protocols were performed in strict accordance with good animal practices, as described in the Guide for the Use and Care of Laboratory Animals published by the National Institutes of Health.

Results

Prnp^{T187N} mice are highly susceptible to prion infection

To investigate how glycans impact prion conversion, we compared prion infection in WT and *Prnp*^{187N} knockin mice, which express PrP with 0–2 or 0–3 N-linked glycans in the C-terminal globular domain of PrP, respectively. The *Prnp*^{187N} mice have a third glycan at position 187 (mouse PrP numbering) from a single amino acid substitution (T187N) that creates a novel N-linked glycan sequon (NXS or NXT) (TVT to NVT) [54] (Fig. 1A). The glycan is located at the C-terminal end of helix 2, nearly equidistant between the two physiological glycans at positions 180 and 196 [54] (Fig. 1A, B).

We previously found that *Prnp*^{187N} and WT mice express equivalent PrP^C levels in the brain [54]. The additional glycan altered PrP^{187N} electrophoretic migration by approximately 2 kDa (Fig. 1C). PrP^{187N} was more highly glycosylated with significantly lower levels of the unglycosylated PrP glycoform (Fig. 1C). To measure PrP^C shed from the cell surface by

ADAM10, we used a newly developed antibody (sPrP^{G228}) that specifically recognizes the new C-terminal epitope generated upon proteolytic cleavage [35], and found a 1.6-fold decrease in cleaved PrP^C, indicating reduced shedding of triglycosylated PrP^C from the cell surface (Fig. 1C). Hence, in contrast to WT PrP^C, where the fully (di-) glycosylated form is the predominant substrate for ADAM10 (Fig. 1C) [35], an additional third glycan at position 187 impairs this cleavage, possibly due to steric hindrance.

To determine how a third glycan would impact prion conversion, neurodegeneration, and survival time, we inoculated mice intracerebrally with four distinct subfibrillar, mouse-adapted prion strains. On first passage, *Prnp*^{187N} mice showed a 100% attack rate, but a markedly prolonged survival period compared to the WT mice (Fig. 2A, Table 1). However, by the second or third passage, three of four strains no longer showed a difference in survival time, indicating that the third glycan made little difference in conversion once the strain was adapted. For the RML-infected mice, the *Prnp*^{187N} mice survived approximately 20% longer than WT mice (WT: 144 ± 5 days; *Prnp*^{187N}: 173 ± 5 days). The variance in the survival times among the *Prnp*^{187N} mice infected with four prion strains was also similar to the WT mice (*Prnp*^{187N}: 155 – 207 days; WT: 140 – 205 days).

To assess how the third glycan affects the severity and regional distribution of neurodegeneration and gliosis, we scored eight brain regions for spongiform degeneration, gliosis, and PrP^{Sc} deposition. Interestingly, RML-infected *Prnp*^{187N} and WT brains displayed similar diffuse aggregate morphology (Fig. 2B) and the lesion profiles were nearly overlapping (Fig. 2C), despite a 30-day difference in the incubation period. The 22L-infected *Prnp*^{187N} brains also showed lesions that were nearly identical to WT (Fig. 2C). However, in *Prnp*^{187N} mice infected with ME7 or mNS prions, there was a consistent decrease in the lesion severity, although the brain regions targeted were unchanged (Fig. 2B, 2C). The primary difference was a profound increase in the size of the plaque-like structures in the *Prnp*^{187N} brains infected with ME7 prions [average plaque diameter 34 ± 2 μm (WT) versus 97 ± 6 μm (*Prnp*^{187N})] and mNS prions [average plaque diameter 34 ± 2 μm (WT) versus 66 ± 6 μm (*Prnp*^{187N})] (Fig. 2B).

ME7 and mNS prions typically form plaque-like structures and accumulate perineuronally in WT mice [39]. We found that the cell tropism was similar in *Prnp*^{187N} mice, as prions from either strain also accumulated perineuronally. Yet exclusively in the *Prnp*^{187N} mice, neurons showed a prominent piling of prion aggregates extending outward from the surface, sometimes obscuring the neuron, suggesting a difference in the aggregate arrangement of highly glycosylated PrP (Fig. 2B). PrP^{Sc} also frequently accumulated along the subarachnoid space and ventricular surfaces in the *Prnp*^{187N} mice, potentially indicating PrP^{Sc} transit through the interstitial fluid. Neuronal and meningeal aggregates were non-congophilic (Figs. 2D and S1) and periventricular aggregates were only rarely and focally congophilic (Fig. S1). To determine whether the PrP^{Sc} was associated with extracellular vesicles (EVs), we co-immunolabelled brain sections for PrP and the tetraspanin and EV marker, CD9 (Fig. S2). Although PrP did not co-localize with CD9 in the WT mice, interestingly, there were focal PrP deposits that co-labelled with CD9 in the *Prnp*^{187N} mice infected with ME7 or mNS prions, particularly periventricularly, suggesting that a subset of 187N-PrP^{Sc} may be attached to EVs.

Triglycosylated PrP^{Sc} is largely GPI-anchored and sediments slowly

We assessed the PrP^{Sc} glycoform ratios by western blot and found that (1) all four strains converted tri-glycosylated PrP into PK-resistant PrP^{Sc} (Fig. 3A), and (2) unglycosylated PrP^{Sc} levels were significantly lower for *Prnp*^{187N} strains than for WT strains (Fig. 3A), potentially due to the lower levels of unglycosylated PrP^C (Fig. 1C).

We previously found that mCWD plaques were enriched in ADAM10-cleaved PrP^{Sc}. To determine the levels of ADAM10-cleaved PrP^{Sc} in ME7- and mNS-infected *Prnp*^{187N} and WT brain, we immunoblotted PK-cleaved brain proteins using the sPrP^{G228} antibody. We found that the cleaved PrP^{Sc} levels were consistently lower by more than a log-fold as compared to mCWD, suggesting that PrP^{Sc} in ME7- and mNS-infected brains remained largely GPI-anchored (Fig. 3B).

To next test whether the prions were internally cleaved as observed in genetic prion disease associated with the F198S-*PRNP* mutation, we probed PK-resistant PrP^{Sc} with a series of antibodies against N- and C-terminal epitopes in PrP. However, no short internal fragments were evident for the ME7 strain, as the highly PK-resistant unglycosylated core fragment was consistently full length and the same molecular weight as WT PrP^{Sc} (Fig. 3C), indicating that PrP was likely to be largely GPI-anchored and not a PrP fragment.

The glycans attached to PrP may impair fibril formation, restricting PrP^{Sc} to small aggregates. To probe the sedimentation properties of highly glycosylated PrP^{Sc}, we performed velocity sedimentation on mNS- and ME7-infected brain samples, both of which displayed alterations in plaque morphology and lesion profiles in the *Prnp*^{187N} mice. We also performed velocity sedimentation on RML-infected brain, in order to include a strain that was not altered by the additional glycan. Brain homogenate was solubilized in a sarcosyl-based buffer, overlaid onto a 4–24% OptiprepTM step gradient, and centrifuged at 150,000 g. Interestingly, the tri-glycosylated mNS and ME7 prions sedimented in lighter fractions than the WT mNS and ME7 prions (Fig. 3D), suggesting that the tri-glycosylated mNS and ME7 prion aggregates were smaller or less compact than the less glycosylated WT prions. Additionally, the PrP^{187N} aggregates were notably more homogenous and nearly monodispersed, as compared to the polydispersed particles in WT mice. By comparison, the RML prion particles from both mouse lines sedimented similarly (Fig 3D).

Triglycosylated PrP^{Sc} binds low levels of heparan sulfate

Glycosaminoglycans, including heparan sulfate (HS), co-localize with prion plaques in the brain [37, 58, 59] and accelerate prion conversion *in vitro* [71]. Unglycosylated PrP has a high heparin binding affinity and frequently forms HS-enriched congophilic plaques [54]. Since the PrP^{187N} aggregates formed non-congophilic, plaque-like deposits in the ME7- and mNS-infected mice, we next tested whether these prions bind HS. Using the antibody 10E4 that binds an N-sulfated glucosamine residue, we immunolabelled ME7 and mNS prion-infected brain sections for HS (Fig 4A). Surprisingly, HS did not co-localize with the PrP plaque-like deposits in the *Prnp*^{187N}-infected brain.

To confirm the lack of HS-PrP binding, we used liquid chromatography - mass spectrometry to quantify the HS levels and determine the HS composition bound to PrP^{Sc} from the ME7-

infected mice (Fig 4B). We purified PrP^{Sc} from WT and *Prnp*^{187N} brains, measured PrP^{Sc} levels compared to a dilution series of recombinant PrP by western blot (Fig. S3), assessed purity by silver stain, and then denatured and degraded the proteins by hydrolysis and enzyme digestion. HS was then purified and aniline tagged, and HS disaccharides were quantified by mass spectrometry compared to standards. We purified PrP^{Sc} from *Prnp*^{180Q,196Q} brains, which have previously been shown to bind high levels of HS, to include as a positive control [54]. The amount of HS bound to PrP^{Sc} from *Prnp*^{187N} brains was not significantly different from WT, and both contained less HS than the PrP^{Sc} purified from *Prnp*^{180Q,196Q} brains. Additionally, the sulfation pattern of the HS bound to PrP^{Sc} in all three samples was not significantly different.

Collectively, this data indicates that ME7 and mNS prions in *PrP*^{187N} mice form plaque-like deposits that are primarily GPI-anchored, Congo red negative, and HS-deficient, consistent with previous findings suggesting that HS does not bind highly glycosylated or GPI-anchored prions with high affinity, and with findings indicating that plaque-like structures observed in sporadic CJD maintain their GPI anchor [73].

Discussion

N-linked glycans stabilize proteins [15, 20, 44], including PrP, and slow prion fibril formation *in vitro* [7]. Here we tested whether the addition of a third glycan to PrP would slow prion disease progression *in vivo*, using *Prnp*^{187N} knockin mice infected with four distinct prion strains. Our results instead demonstrate that *Prnp*^{187N} mice remain highly susceptible to prions and show minimal changes in survival times, indicating that the additional glycan did not significantly hinder prion conversion.

The histopathology was markedly altered in the brains of *Prnp*^{187N} mice infected with two of four prion strains, ME7 and mNS. PrP^{Sc} typically accumulates as a thin band along neuronal cell membranes and as small plaque-like aggregates in WT mice. Instead, ME7 and mNS prions formed an extensive assembly of PrP^{Sc} emerging from neuronal surfaces. These large plaque-like deposits differ from true amyloid plaques, as deposits were cell-associated, likely GPI-anchored, non-congophilic, and had low levels of bound HS. Notably, *Prnp*^{180Q,196Q} mice expressing unglycosylated PrP develop a starkly different disease phenotype following ME7 and mNS infection, forming congophilic plaques composed of ADAM10-cleaved PrP highly enriched in HS [54]. Collectively, these results indicate that certain prions can switch between true amyloid plaques and cell-associated plaque-like deposits, depending on the number of N-linked glycans on PrP^C (zero or three). The subtle amino acid differences are unlikely to underlie the strain switch, as Tuzi and colleagues found that ME7 prion-infected *Prnp*^{180T,196T} knockin mice, which also express unglycosylated PrP, similarly formed amyloid plaques [64].

Prion glycosylation inversely correlates with PrP^{Sc}-bound heparan sulfate

Interestingly, early reports indicate that non-plaque deposits immunolabel minimally for HS, whereas amyloid plaques immunolabel strongly for HS in mice and in humans [1, 54, 59]. Indeed, previously we found that plaque formation and prion-bound HS levels measured by LC/MS were highly correlated [1, 54]. Here, none of the four strains in the *Prnp*^{187N} mice

formed plaques enriched in HS, as had occurred in the *Prnp*^{180Q,196Q} mice. Although *Prnp*^{187N} mice infected with two strains formed plaque-like aggregates, prion-bound HS levels were low, in agreement with previous findings that the N-linked glycans reduce the PrP binding affinity to sulfated glycosaminoglycans [54]. Collectively, these results, together with previous data in mice and in humans, reinforce the concept that glycans diminish PrP interaction with HS co-factors that could aid in scaffolding fibril formation, which may be limiting glycosylated prions to oligomers.

PrP glycans promote aggregation on membranes to form large plaque-like structures

GPI-anchoring of PrP hinders fibril formation, as mice expressing GPI-anchorless PrP consistently develop amyloid fibrils perivascularly following infection with diverse prion strains [2, 14]. These findings, together with observations in human genetic prion disease associated with GPI-anchorless PrP [22–24], have led to the suggestion that the GPI-anchor modulates fibril assembly of PrP, potentially through steric interference of fibril formation. To this end, a GPI-anchored form of the yeast prion, Sup35, expressed in neuronal cells formed membrane-bound, nonfibrillar aggregates, whereas GPI-anchorless Sup35 formed fibrils [36]. Interestingly, Sup35 accumulated in extracellular vesicles piling on the cell surface, which may be relevant to our findings of extensive plaque-like deposits of ME7 and mNS prions piling on neuronal cell membranes. Considering that prions can be converted on the plasma membrane or in multivesicular bodies (MVB) [11, 72], it is conceivable that ME7 and mNS prions accumulate in extracellular vesicles (EVs) (microvesicles or exosomes) that are trapped on the cell membrane. In this case, prions would retain the GPI-anchor, but would also be mobile and could transit through the interstitial and cerebrospinal fluid, accumulating periventricularly and adjacent to meninges, as we observed with PrP^{Sc} and CD9 co-localization. In support of this possibility, EVs have been shown to harbor prion aggregates and facilitate prion spread [21, 67].

Previously PrP^{Sc} was thought to retain the GPI-anchor, however, not all prions are exclusively GPI-anchored. For example, a plaque-forming prion, mCWD, is composed of monoglycosylated, shed PrP that lacks the GPI-anchor [1]. In humans with sporadic CJD, the presence of the GPI-anchor on plaque-like prion deposits has been controversial [40, 73], with recent biochemical evidence indicating that sCJD deposits are composed of GPI-anchored PrP [73]. Taken together, our data suggest that multiple N-linked glycans on PrP favor the conversion of GPI-anchored small or compact oligomers that bind poorly to HS, and accumulate as diffuse and plaque-like deposits associated with cells and at sites of interstitial and CSF efflux. Future studies to determine whether the plaque-like deposits originate from surface-associated microvesicles budding from the cell surface, from released MVB-derived exosomes, or from another source, will provide insight into subcellular prion conversion sites and the rapid dissemination of human and animal prions.

Supplementary Material

Refer to Web version on PubMed Central for supplementary material.

Acknowledgements

We thank Jin Wang and Taylor Winrow for outstanding technical support, and the animal care staff at UC San Diego for excellent animal care. We thank the UC San Diego GlycoAnalytics Core for the mass spectrometry analysis, and Dr. Patricia Aguilar-Calvo for critical review of the manuscript. This study was supported by the National Institutes of Health grants NS069566 (CJS), NS076896 (CJS), CJD Foundation (CJS and HCA), and the Werner-Otto-Stiftung (HCA). This work was also supported by the National Heart, Lung, and Blood Institute of the National Institutes of Health under K12HL141956 (JAC).

References

1. Aguilar-Calvo P, Sevillano AM, Bapat J, Soldau K, Sandoval DR, Altmepfen HC, Linsenmeier L, Pizzo DP, Geschwind MD, Sanchez Het al. (2019) Shortening heparan sulfate chains prolongs survival and reduces parenchymal plaques in prion disease caused by mobile, ADAM10-cleaved prions. *Acta Neuropathol*: Doi 10.1007/s00401-019-02085-x
2. Aguilar-Calvo P, Xiao X, Bett C, Erana H, Soldau K, Castilla J, Nilsson KP, Surewicz WK, Sigurdson CJ (2017) Post-translational modifications in PrP expand the conformational diversity of prions in vivo. *Sci Rep* 7: 43295 Doi 10.1038/srep43295 [PubMed: 28272426]
3. Aguzzi A, Lakkaraju AK (2016) Cell Biology of Prions and Prionoids: A Status Report. *Trends Cell Biol* 26: 40–51 Doi 10.1016/j.tcb.2015.08.007 [PubMed: 26455408]
4. Baiardi S, Rossi M, Capellari S, Parchi P (2019) Recent advances in the histo-molecular pathology of human prion disease. *Brain Pathol* 29: 278–300 Doi 10.1111/bpa.12695 [PubMed: 30588685]
5. Baldwin MA, Stahl N, Reinders LG, Gibson BW, Prusiner SB, Burlingame AL (1990) Permethylated and tandem mass spectrometry of oligosaccharides having free hexosamine: analysis of the glycoinositol phospholipid anchor glycan from the scrapie prion protein. *Anal Biochem* 191: 174–182 [PubMed: 1981823]
6. Baron GS, Hughson AG, Raymond GJ, Offerdahl DK, Barton KA, Raymond LD, Dorward DW, Caughey B (2011) Effect of glycans and the glycoposphatidylinositol anchor on strain dependent conformations of scrapie prion protein: improved purifications and infrared spectra. *Biochemistry* 50: 4479–4490 Doi 10.1021/bi2003907 [PubMed: 21539311]
7. Bosques CJ, Imperiali B (2003) The interplay of glycosylation and disulfide formation influences fibrillization in a prion protein fragment. *Proc Natl Acad Sci U S A* 100: 7593–7598 Doi 10.1073/pnas.1232504100 [PubMed: 12805563]
8. Bruce ME (1993) Scrapie strain variation and mutation. *Br Med Bull* 49: 822–838 [PubMed: 8137131]
9. Bruce ME, Dickinson AG (1979) Biological stability of different classes of scrapie agent. In *Slow Virus Infections of the Central Nervous System* In: Prusiner SB, Hadlow WH (eds) In *Slow Virus Infections of the Central Nervous System*. New York: Academic Press, City, pp 71–86
10. Burke CM, Walsh DJ, Steele AD, Agrimi U, Di Bari MA, Watts JC, Supattapone S (2019) Full restoration of specific infectivity and strain properties from pure mammalian prion protein. *PLoS Pathog* 15: e1007662 Doi 10.1371/journal.ppat.1007662 [PubMed: 30908557]
11. Caughey B, Raymond GJ, Ernst D, Race RE (1991) N-terminal truncation of the scrapie-associated form of PrP by lysosomal protease(s): implications regarding the site of conversion of PrP to the protease-resistant state. *J Virol* 65: 6597–6603 [PubMed: 1682507]
12. Caughey BW, Dong A, Bhat KS, Ernst D, Hayes SF, Caughey WS (1991) Secondary structure analysis of the scrapie-associated protein PrP 27–30 in water by infrared spectroscopy [published erratum appears in *Biochemistry* 1991 Oct 29;30(43):10600]. *Biochemistry* 30: 7672–7680 [PubMed: 1678278]
13. Chesebro B, Race R, Wehrly K, Nishio J, Bloom M, Lechner D, Bergstrom S, Robbins K, Mayer L, Keith JM (1985) Identification of scrapie prion protein-specific mRNA in scrapie-infected and uninfected brain. *Nature* 315: 331–333 [PubMed: 3923361]
14. Chesebro B, Trifilo M, Race R, Meade-White K, Teng C, LaCasse R, Raymond L, Favara C, Baron G, Priola Set al. (2005) Anchorless prion protein results in infectious amyloid disease without clinical scrapie. *Science* 308: 1435–1439 [PubMed: 15933194]

15. Culyba EK, Price JL, Hanson SR, Dhar A, Wong CH, Gruebele M, Powers ET, Kelly JW (2011) Protein native-state stabilization by placing aromatic side chains in N-glycosylated reverse turns. *Science* 331: 571–575 Doi 10.1126/science.1198461 [PubMed: 21292975]
16. Deleault NR, Harris BT, Rees JR, Supattapone S (2007) Formation of native prions from minimal components in vitro. *Proc Natl Acad Sci U S A* 104: 9741–9746 [PubMed: 17535913]
17. Dickinson AG (1976) Scrapie in sheep and goats. *Front Biol* 44: 209–241 [PubMed: 821790]
18. Dickinson AW, Outram GW, Taylor DM, Foster JD (1986) Further evidence that scrapie agent has an independent genome In: In Court LA, Dormont D, Brown P, Kingsbury DT (eds) *Unconventional Virus Diseases of the Central Nervous System*. Commisariat à l’Energie Atomique, Paris, France, City, pp 446–460
19. Endo T, Groth D, Prusiner SB, Kobata A (1989) Diversity of oligosaccharide structures linked to asparagines of the scrapie prion protein. *Biochemistry* 28: 8380–8388 [PubMed: 2574992]
20. Feng X, Wang X, Han B, Zou C, Hou Y, Zhao L, Li C (2018) Design of Glyco-Linkers at Multiple Structural Levels to Modulate Protein Stability. *J Phys Chem Lett* 9: 4638–4645 Doi 10.1021/acs.jpcclett.8b01570 [PubMed: 30060662]
21. Fevrier B, Vilette D, Archer F, Loew D, Faigle W, Vidal M, Laude H, Raposo G (2004) Cells release prions in association with exosomes. *Proc Natl Acad Sci U S A* 101: 9683–9688 [PubMed: 15210972]
22. Ghetti B, Piccardo P, Frangione B, Bugiani O, Giaccone G, Young K, Prelli F, Farlow MR, Dlouhy SR, Tagliavini F (1996) Prion Protein Amyloidosis. *Brain Pathol* 6: 127–145 [PubMed: 8737929]
23. Ghetti B, Piccardo P, Frangione B, Bugiani O, Giaccone G, Young K, Prelli F, Farlow MR, Dlouhy SR, Tagliavini F (1996) Prion Protein Hereditary Amyloidosis - Parenchymal and Vascular. *Semin Virol* 7: 189–200
24. Ghetti B, Piccardo P, Spillantini MG, Ichimiya Y, Porro M, Perini F, Kitamoto T, Tateishi J, Seiler C, Frangione B et al. (1996) Vascular variant of prion protein cerebral amyloidosis with tau-positive neurofibrillary tangles: the phenotype of the stop codon 145 mutation in PRNP. *Proc Natl Acad Sci U S A* 93: 744–748 [PubMed: 8570627]
25. Ghetti B, Piccardo P, Zanuso G (2018) Dominantly inherited prion protein cerebral amyloidoses - a modern view of Gerstmann-Straussler-Scheinker. *Handb Clin Neurol* 153: 243–269 Doi 10.1016/b978-0-444-63945-5.00014-3 [PubMed: 29887140]
26. Greenlee JJ, Greenlee MH (2015) The transmissible spongiform encephalopathies of livestock. *ILAR journal* 56: 7–25 Doi 10.1093/ilar/ilv008 [PubMed: 25991695]
27. Group. W (2020) GLYCAM Web. Complex Carbohydrate Research Center <http://glycam.org>
28. Iwasaki Y, Kato H, Ando T, Mimuro M, Kitamoto T, Yoshida M (2017) MM1-type sporadic Creutzfeldt-Jakob disease with 1-month total disease duration and early pathologic indicators. *Neuropathology* 37: 420–425 Doi 10.1111/neup.12379 [PubMed: 28402042]
29. Jucker M, Walker LC (2018) Propagation and spread of pathogenic protein assemblies in neurodegenerative diseases. *Nat Neurosci* 21: 1341–1349 Doi 10.1038/s41593-018-0238-6 [PubMed: 30258241]
30. Katorcha E, Baskakov IV (2017) Analyses of N-linked glycans of PrP(Sc) revealed predominantly 2,6-linked sialic acid residues. *FEBS J* 284: 3727–3738 Doi 10.1111/febs.14268 [PubMed: 28898525]
31. Kim MO, Takada LT, Wong K, Forner SA, Geschwind MD (2018) Genetic PrP Prion Diseases. *Cold Spring Harb Perspect Biol* 10: Doi 10.1101/cshperspect.a033134
32. Kovacs GG (2019) Molecular pathology of neurodegenerative diseases: principles and practice. *J Clin Pathol* 72: 725–735 Doi 10.1136/jclinpath-2019-205952 [PubMed: 31395625]
33. Lawrence R, Brown JR, Al-Mafraji K, Lamanna WC, Beitel JR, Boons GJ, Esko JD, Crawford BE (2012) Disease-specific non-reducing end carbohydrate biomarkers for mucopolysaccharidoses. *Nat Chem Biol* 8: 197–204 Doi nchembio.766 [pii] 10.1038/nchembio.766 [PubMed: 22231271]
34. Lawrence R, Olson SK, Steele RE, Wang L, Warrior R, Cummings RD, Esko JD (2008) Evolutionary differences in glycosaminoglycan fine structure detected by quantitative glycan reductive isotope labeling. *J Biol Chem* 283: 33674–33684 Doi 10.1074/jbc.M804288200 [PubMed: 18818196]

35. Linsenmeier L, Mohammadi B, Wetzel S, Puig B, Jackson WS, Hartmann A, Uchiyama K, Sakaguchi S, Endres K, Tatzelt J et al. (2018) Structural and mechanistic aspects influencing the ADAM10-mediated shedding of the prion protein. *Mol Neurodegener* 13: 18 Doi 10.1186/s13024-018-0248-6 [PubMed: 29625583]
36. Marshall KE, Offerdahl DK, Speare JO, Dorward DW, Hasenkrug A, Carmody AB, Baron GS (2014) Glycosylphosphatidylinositol anchoring directs the assembly of Sup35NM protein into non-fibrillar, membrane-bound aggregates. *J Biol Chem* 289: 12245–12263 Doi 10.1074/jbc.M114.556639 [PubMed: 24627481]
37. McBride PA, Wilson MI, Eikelenboom P, Tunstall A, Bruce ME (1998) Heparan sulfate proteoglycan is associated with amyloid plaques and neuroanatomically targeted PrP pathology throughout the incubation period of scrapie-infected mice. *Exp Neurol* 149: 447–454 [PubMed: 9500966]
38. Mitra N, Sinha S, Ramya TN, Surolia A (2006) N-linked oligosaccharides as outfitters for glycoprotein folding, form and function. *Trends Biochem Sci* 31: 156–163 Doi 10.1016/j.tibs.2006.01.003 [PubMed: 16473013]
39. Nilsson KP, Joshi-Barr S, Winson O, Sigurdson CJ (2010) Prion strain interactions are highly selective. *J Neurosci* 30: 12094–12102 Doi 10.1523/JNEUROSCI.2417-10.2010 [PubMed: 20826672]
40. Notari S, Strammiello R, Capellari S, Giese A, Cescatti M, Grassi J, Ghetti B, Langeveld JP, Zou WQ, Gambetti P et al. (2008) Characterization of truncated forms of abnormal prion protein in Creutzfeldt-Jakob disease. *J Biol Chem* 283: 30557–30565 Doi 10.1074/jbc.M801877200 [PubMed: 18753138]
41. Oesch B, Westaway D, Walchli M, McKinley MP, Kent SB, Aebersold R, Barry RA, Tempst P, Teplow DB, Hood LE et al. (1985) A cellular gene encodes scrapie PrP 27–30 protein. *Cell* 40: 735–746 [PubMed: 2859120]
42. Peretz D, Scott MR, Groth D, Williamson RA, Burton DR, Cohen FE, Prusiner SB (2001) Strain-specified relative conformational stability of the scrapie prion protein. *Protein Sci* 10: 854–863 [PubMed: 11274476]
43. Polymenidou M, Moos R, Scott M, Sigurdson C, Shi YZ, Yajima B, Hafner-Bratkovic I, Jerala R, Hornemann S, Wuthrich K et al. (2008) The POM monoclonals: a comprehensive set of antibodies to non-overlapping prion protein epitopes. *PLoS One* 3: e3872 Doi 10.1371/journal.pone.0003872 [PubMed: 19060956]
44. Price JL, Culyba EK, Chen W, Murray AN, Hanson SR, Wong CH, Powers ET, Kelly JW (2012) N-glycosylation of enhanced aromatic sequons to increase glycoprotein stability. *Biopolymers* 98: 195–211 Doi 10.1002/bip.22030 [PubMed: 22782562]
45. Price JL, Powers DL, Powers ET, Kelly JW (2011) Glycosylation of the enhanced aromatic sequon is similarly stabilizing in three distinct reverse turn contexts. *Proc Natl Acad Sci U S A* 108: 14127–14132 Doi 10.1073/pnas.1105880108 [PubMed: 21825145]
46. Prusiner SB (1982) Novel proteinaceous infectious particles cause scrapie. *Science* 216: 136–144 [PubMed: 6801762]
47. Prusiner SB, Scott M, Foster D, Pan KM, Groth D, Mirenda C, Torchia M, Yang SL, Serban D, Carlson GA et al. (1990) Transgenic studies implicate interactions between homologous PrP isoforms in scrapie prion replication. *Cell* 63: 673–686 [PubMed: 1977523]
48. Raymond GJ, Chabry J (2004) Methods and Tools in Biosciences and Medicine. In: Lehmann S, Grassi J (eds) *Techniques in Prion Research*. Birkhäuser, Basel, City, pp 16–26
49. Riek R, Hornemann S, Wider G, Billeter M, Glockshuber R, Wuthrich K (1996) Nmr Structure of the Mouse Prion Protein Domain Prp(121–231). *Nature* 382: 180–182 [PubMed: 8700211]
50. Rudd PM, Endo T, Colominas C, Groth D, Wheeler SF, Harvey DJ, Wormald MR, Serban H, Prusiner SB, Kobata A et al. (1999) Glycosylation differences between the normal and pathogenic prion protein isoforms. *Proc Natl Acad Sci U S A* 96: 13044–13049 [PubMed: 10557270]
51. Rudd PM, Wormald MR, Wing DR, Prusiner SB, Dwek RA (2001) Prion glycoprotein: structure, dynamics, and roles for the sugars. *Biochemistry* 40: 3759–3766 [PubMed: 11300755]

52. Sandberg MK, Al-Doujaily H, Sharps B, Clarke AR, Collinge J (2011) Prion propagation and toxicity in vivo occur in two distinct mechanistic phases. *Nature* 470: 540–542 Doi 10.1038/nature09768 [PubMed: 21350487]
53. Selkoe DJ (1991) The molecular pathology of Alzheimer's disease. *Neuron* 6: 487–498 [PubMed: 1673054]
54. Sevillano AM, Aguilar-Calvo P, Kurt TD, Lawrence JA, Soldau K, Nam TH, Schumann T, Pizzo DP, Nystrom S, Choudhury B et al. (2020) Prion protein glycans reduce intracerebral fibril formation and spongiosis in prion disease. *J Clin Invest*: Doi 10.1172/jci131564
55. Sigurdson CJ, Manco G, Schwarz P, Liberski P, Hoover EA, Hornemann S, Polymenidou M, Miller MW, Glatzel M, Aguzzi A (2006) Strain fidelity of chronic wasting disease upon murine adaptation. *J Virol* 80: 12303–12311 Doi 10.1128/jvi.01120-06 [PubMed: 17020952]
56. Sim VL, Caughey B (2008) Ultrastructures and strain comparison of under-glycosylated scrapie prion fibrils. *Neurobiol Aging*: Doi S0197-4580(08)00065-1 [pii] 10.1016/j.neurobiolaging.2008.02.016
57. Snow AD, Kisilevsky R, Willmer J, Prusiner SB, DeArmond SJ (1989) Sulfated glycosaminoglycans in amyloid plaques of prion diseases. *Acta Neuropathol* 77: 337–342 [PubMed: 2523631]
58. Snow AD, Kisilevsky R, Willmer J, Prusiner SB, DeArmond SJ (1989) Sulfated glycosaminoglycans in amyloid plaques of prion diseases. *Acta Neuropathol Berl* 77: 337–342 [PubMed: 2523631]
59. Snow AD, Wight TN, Nochlin D, Koike Y, Kimata K, DeArmond SJ, Prusiner SB (1990) Immunolocalization of heparan sulfate proteoglycans to the prion protein amyloid plaques of Gerstmann-Straussler syndrome, Creutzfeldt-Jakob disease and scrapie. *Lab Invest* 63: 601–611 [PubMed: 1977959]
60. Srivastava S, Katorcha E, Daus ML, Lasch P, Beekes M, Baskakov IV (2017) Sialylation Controls Prion Fate in Vivo. *J Biol Chem* 292: 2359–2368 Doi 10.1074/jbc.M116.768010 [PubMed: 27998976]
61. Srivastava S, Katorcha E, Makarava N, Barrett JP, Loane DJ, Baskakov IV (2018) Inflammatory response of microglia to prions is controlled by sialylation of PrP(Sc). *Sci Rep* 8: 11326 Doi 10.1038/s41598-018-29720-z [PubMed: 30054538]
62. Stahl N, Baldwin MA, Prusiner SB (1991) Electrospray mass spectrometry of the glycosylinositol phospholipid of the scrapie prion protein. *Cell Biol Int Rep* 15: 853–862 [PubMed: 1686992]
63. Stohr J, Weinmann N, Wille H, Kaimann T, Nagel-Steger L, Birkmann E, Panza G, Prusiner SB, Eigen M, Riesner D (2008) Mechanisms of prion protein assembly into amyloid. *Proc Natl Acad Sci U S A* 105: 2409–2414 Doi 10.1073/pnas.0712036105 [PubMed: 18268326]
64. Tuzi NL, Cancellotti E, Baybutt H, Blackford L, Bradford B, Plinston C, Coghill A, Hart P, Piccardo P, Barron RM et al. (2008) Host PrP glycosylation: a major factor determining the outcome of prion infection. *PLoS Biol* 6: e100 Doi 07-PLBI-RA-2655 [pii] 10.1371/journal.pbio.0060100 [PubMed: 18416605]
65. Vaquer-Alicea J, Diamond MI (2019) Propagation of Protein Aggregation in Neurodegenerative Diseases. *Annu Rev Biochem* 88: 785–810 Doi 10.1146/annurev-biochem-061516-045049 [PubMed: 30917002]
66. Varki A (2017) Biological roles of glycans. *Glycobiology* 27: 3–49 Doi 10.1093/glycob/cww086 [PubMed: 27558841]
67. Vella LJ, Sharples RA, Lawson VA, Masters CL, Cappai R, Hill AF (2007) Packaging of prions into exosomes is associated with a novel pathway of PrP processing. *J Pathol* 211: 582–590 Doi 10.1002/path.2145 [PubMed: 17334982]
68. Wadsworth JDF, Joiner S, Hill AF, Campbell TA, Desbruslais M, Luthert PJ, Collinge J. (2001) Tissue distribution of protease resistant prion protein in variant CJD using a highly sensitive immuno-blotting assay. *Lancet* 358: 171–180 [PubMed: 11476832]
69. Wang F, Wang X, Yuan CG, Ma J (2010) Generating a prion with bacterially expressed recombinant prion protein. *Science* 327: 1132–1135 Doi science.1183748 [pii] 10.1126/science.1183748 [PubMed: 20110469]

70. Weerapana E, Imperiali B (2006) Asparagine-linked protein glycosylation: from eukaryotic to prokaryotic systems. *Glycobiology* 16: 91r–101r Doi 10.1093/glycob/cwj099
71. Wong C, Xiong LW, Horiuchi M, Raymond L, Wehrly K, Chesebro B, Caughey B (2001) Sulfated glycans and elevated temperature stimulate PrP(Sc)-dependent cell-free formation of protease-resistant prion protein. *EMBO J* 20: 377–386. [PubMed: 11157745]
72. Yim YI, Park BC, Yadavalli R, Zhao X, Eisenberg E, Greene LE (2015) The multivesicular body is the major internal site of prion conversion. *J Cell Sci* 128: 1434–1443 Doi 10.1242/jcs.165472 [PubMed: 25663703]
73. Zanusso G, Fiorini M, Ferrari S, Meade-White K, Barbieri I, Brocchi E, Ghetti B, Monaco S (2014) Gerstmann-Straussler-Scheinker disease and “anchorless prion protein” mice share prion conformational properties diverging from sporadic Creutzfeldt-Jakob disease. *J Biol Chem* 289: 4870–4881 Doi 10.1074/jbc.M113.531335 [PubMed: 24398683]
74. Zerr I, Parchi P (2018) Sporadic Creutzfeldt-Jakob disease. *Handb Clin Neurol* 153: 155–174 Doi 10.1016/b978-0-444-63945-5.00009-x [PubMed: 29887134]
75. Zerr I, Schulz-Schaeffer WJ, Giese A, Bodemer M, Schroter A, Henkel K, Tschampa HJ, Windl O, Pfahlberg A, Steinhoff B et al. (2000) Current clinical diagnosis in Creutzfeldt-Jakob disease: identification of uncommon variants. *Ann Neurol* 48: 323–329. [PubMed: 10976638]

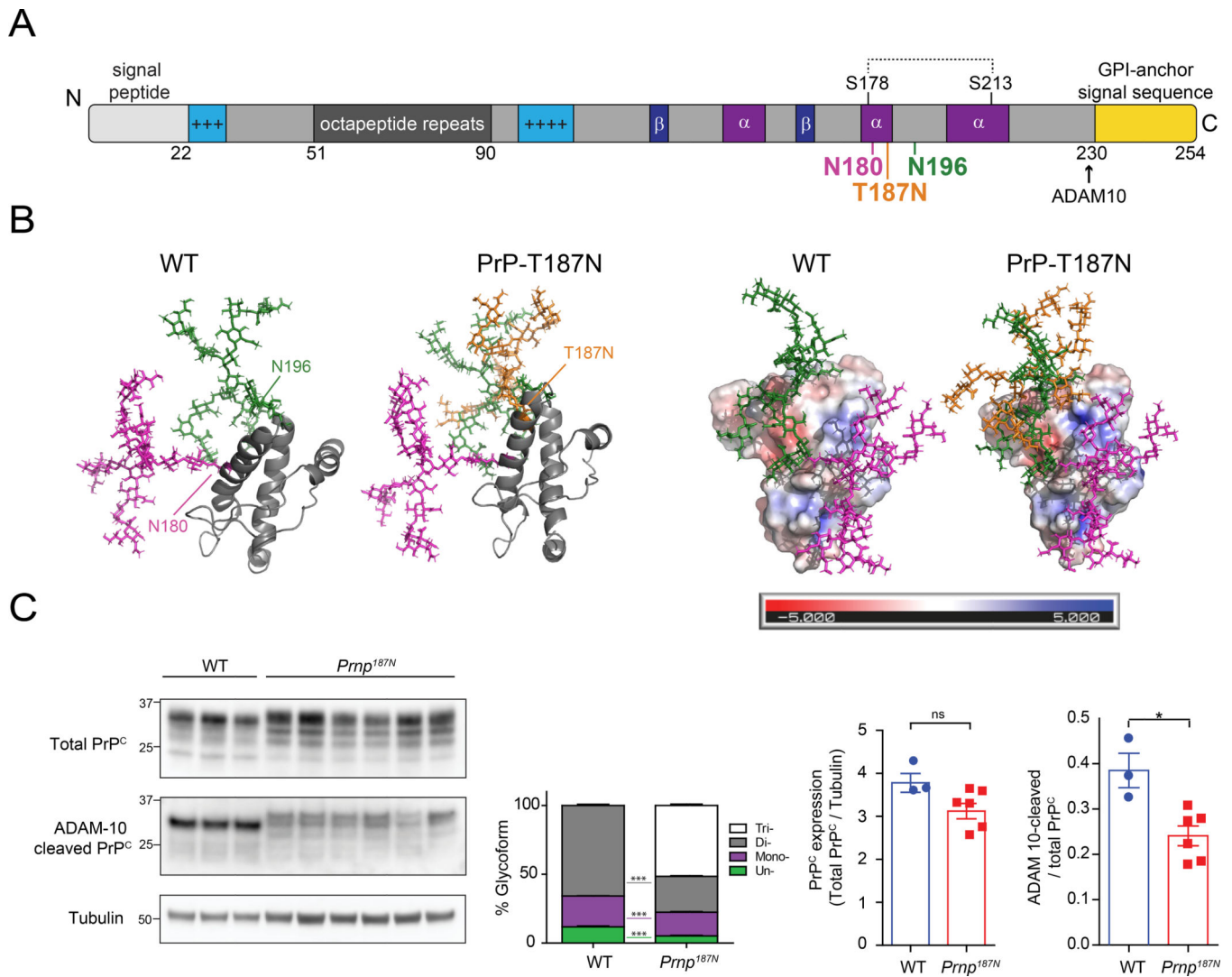


Figure 1. The T187N mutation introduces a third N-linked glycan to the globular C-terminal domain of PrP^C.

A. The PrP^C primary structure shows the positively charged segments (light blue), Cu²⁺-binding octapeptide repeats (dark grey), beta sheets (dark blue), alpha helices (purple), disulfide bonds (dotted line), and GPI-anchor signal sequence (yellow). The glycans are linked to PrP residues 180N and 196N, and to the mutated 187N residue. **B.** Three-dimensional structure of the mature PrP^C protein shown in ribbon form (left) or as a charged surface (right) (PDB ID code 1AG2). N-linked glycans attached to N180, N196, and N187 are depicted in magenta, green, and orange, respectively (note: tetra-antennary, terminally-sialylated glycans are shown [30, 50]). **C.** Western blots (left) show total and ADAM10 cleaved PrP^C protein levels in whole brain lysates from adult WT or *Prnp*^{187N} mice. Graphs indicate relative percentages of each glycoform from total PrP: un- (green), mono- (purple), di- (grey), and tri-glycosylated (white) (mean ± SEM). Also quantified is ADAM10-cleaved PrP. N = 3 – 6 mice per genotype.

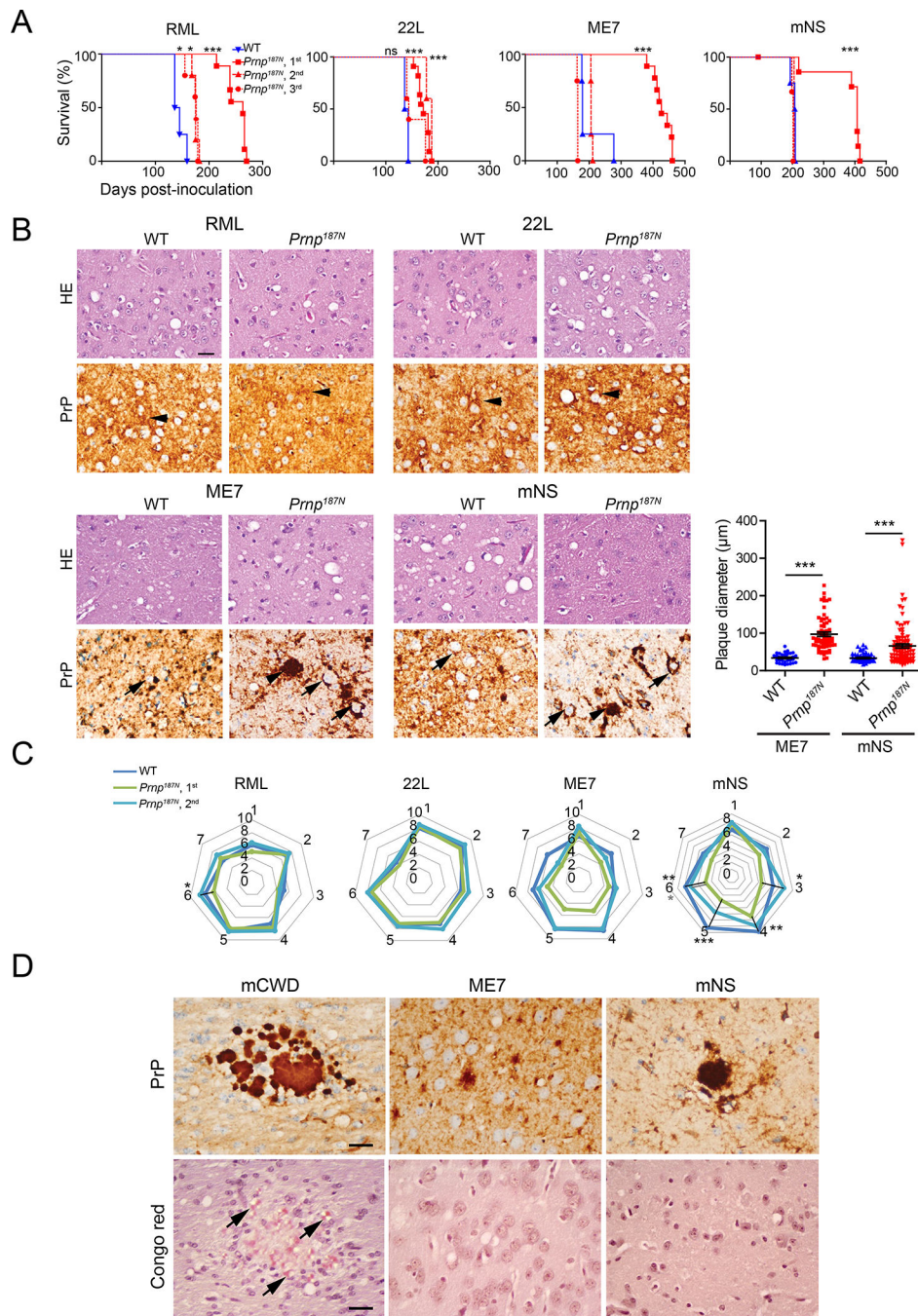


Figure 2. *Prnp^{187N}* mice initially show a prolonged survival time and plaque-like prion deposits in the brain for select strains.

A. Survival curves reveal a delayed time to the onset of terminal disease on the first passage for all strains, which decreased on subsequent passages. **B.** HE and PrP immunostains revealed similar spongiform degeneration and diffuse PrP^{Sc} deposits in the RML and 22L-infected WT and *Prnp^{187N}* mice (arrowheads). Plaque-like deposits (arrowheads) were significantly larger in the ME7- and mNS-infected *Prnp^{187N}* mice. Graph indicates plaque diameter (N=3 mice per group, n = 35 plaques). Note the peri-neuronal prion deposits in the

ME7 and mNS-infected WT and *Prnp*^{187N} brain (arrows). **C.** Lesion profiles indicate the severity of spongiform change, astrogliosis, and PrP^{Sc} deposition in 7 brain areas and are nearly superimposable for RML and 22L-infected WT and *Prnp*^{187N} mice. ME7- and mNS-infected mice showed less severe histopathologic lesions on first passage as compared to WT mice, however lesion severity increased by second passage (1-dorsal medulla, 2-cerebellum, 3-hypothalamus, 4-medial thalamus, 5-hippocampus, 6-cerebral cortex, 7-cerebral peduncles). For panel C: n=4–6 mice/group. **D.** Prion-like ME7 and mNS plaques in the *Prnp*^{187N} brains are largely non-congophilic, unlike the mouse-adapted CWD prion strain (mCWD) used as a positive control. Brain regions shown in B: RML and 22L, cerebral cortex; ME7 and mNS, thalamus, and (D) Congo red stain: mCWD, corpus callosum; ME7 and mNS, cerebral cortex. Scale bar = 50 μ m (panel B). *P< 0.05, **P< 0.01, ***P< 0.001, Log-rank (Mantel-Cox) test (panel A), unpaired t-test (panel B), 2-way ANOVA with Bonferroni post (panel C).

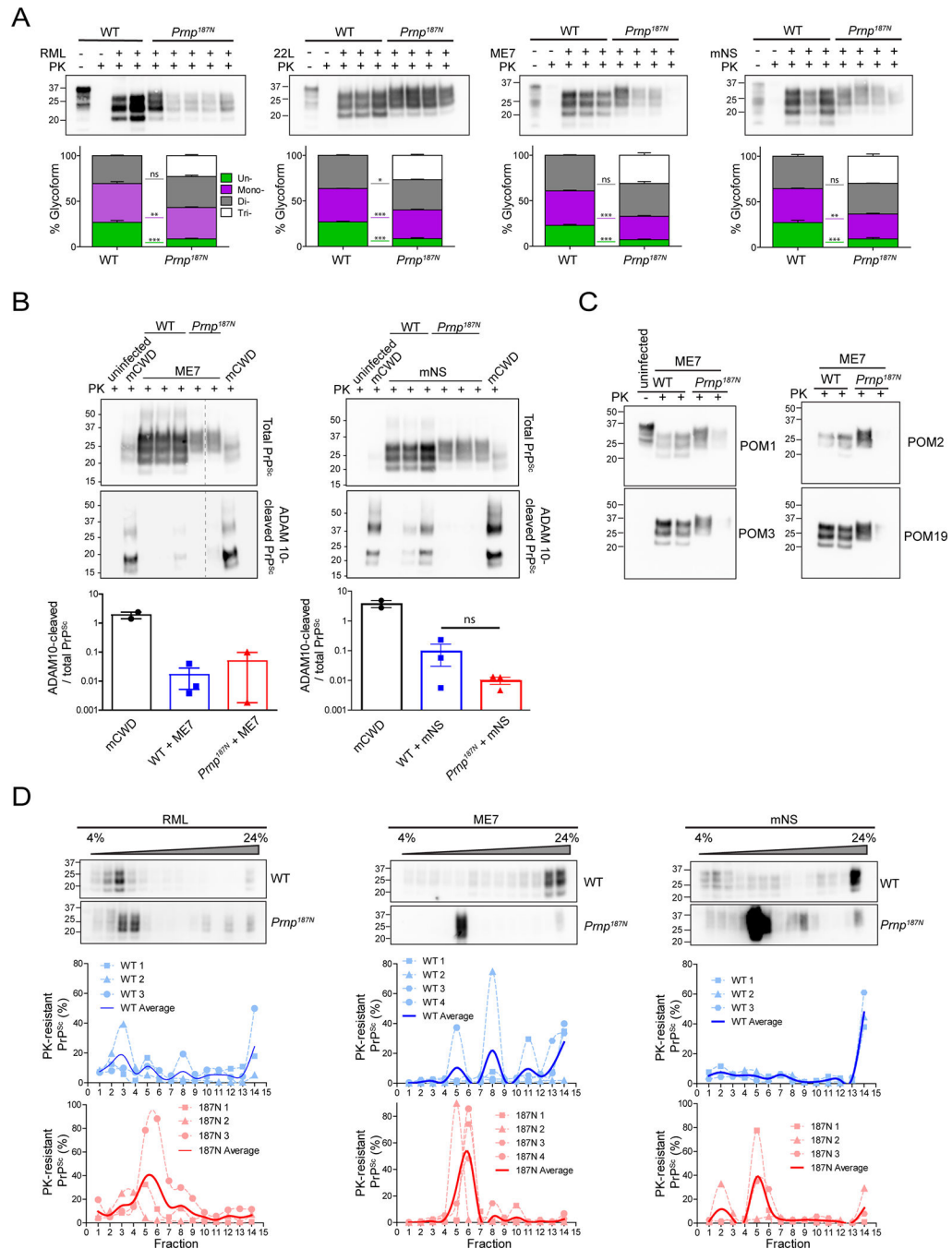


Figure 3. Biochemical properties of 187N-PrP^{Sc}.

A. Electrophoretic mobility and glycoform profile of PrP^{Sc} from RML-, 22L-, ME7-, or mNS-prion-infected brain lysates (upper) show low levels of unglycosylated PrP^{Sc} in the *Pmp*^{187N} mice brain. Lysates were treated with proteinase K (PK) where indicated to degrade PrP^C. Quantification of glycoforms (lower) show percentage of PrP^{Sc} that contains zero (green), one (purple), two (grey), or three glycans (white). **B.** Representative western blots of ME7- or mNS-infected brain lysates from WT or *Pmp*^{187N} mice show total (upper) or ADAM10-cleaved PrP^{Sc} shed from the cell surface (lower). Brain from mCWD-infected

mice contain abundant ADAM10-cleaved PrP^{Sc} (positive control) [54]. Graphs show quantification (mean \pm SE). **C.** Western blots show ME7-infected brain using antibodies against the octapeptide region of the PrP N-terminus (amino acids 53–88) (POM2), amino acids 95–100 (POM3), and a discontinuous epitope that includes the middle and distal C-terminus, which includes amino acid 220 (POM19) [43]. **D.** Western blots from a sedimentation velocity of RML, mNS, or ME7 prion-infected WT or *Prnp*^{I87N} mice overlaid on a 4–24% Opti-prepTM step gradient, with the pellet fraction in the far right lane. Quantifications are shown below. N = 3 – 4 biological replicates per genotype for each strain, except for ME7-infected *Prnp*^{I87N} shown in panel B (N = 2).

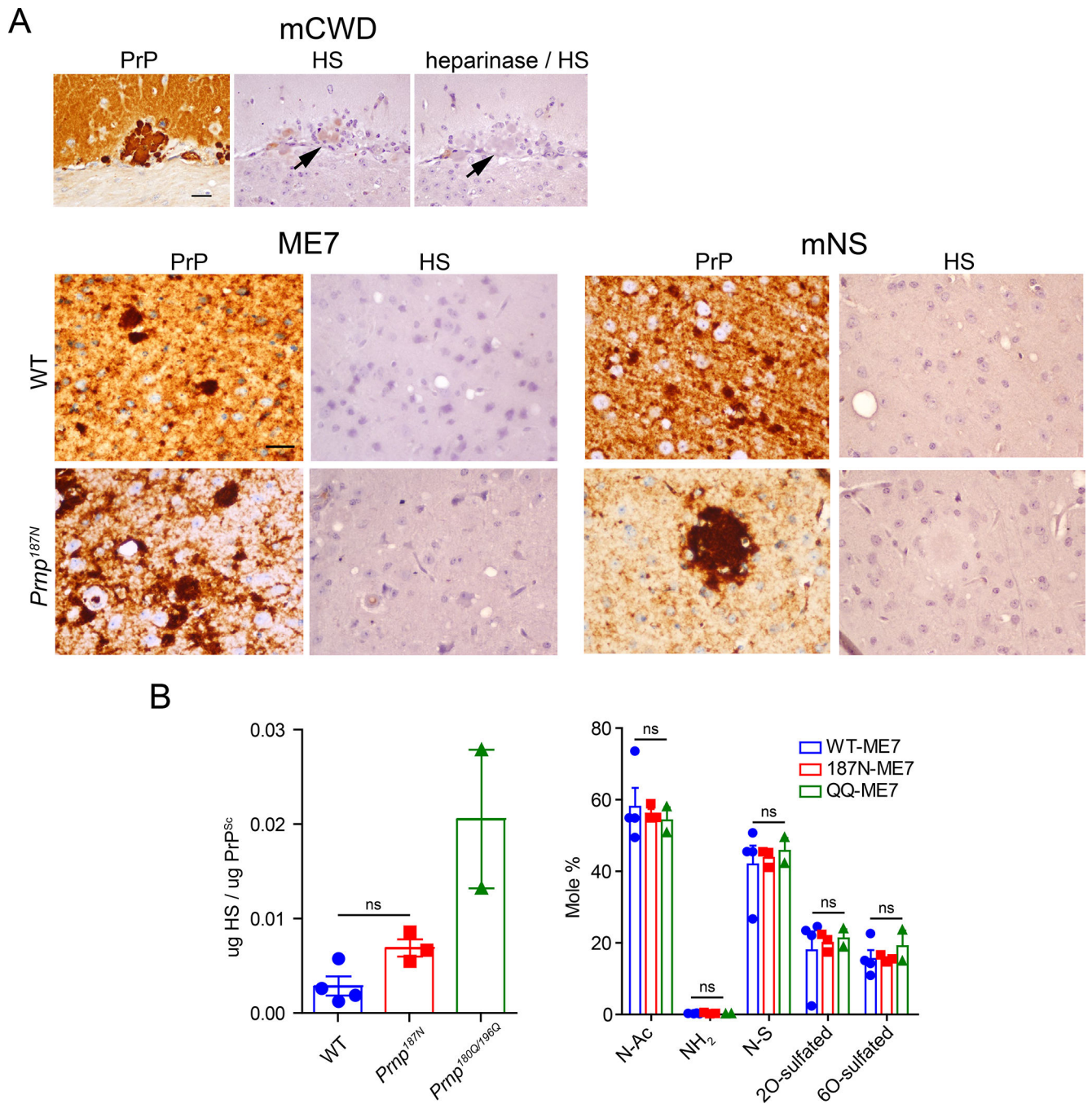


Figure 4. Heparan sulfate binding properties of PrP^{187N}.

A. ME7 and mNS plaque-like deposits in the WT and *Prnp*^{187N} brain sections do not label for HS using the anti-HS antibody 10E4, in contrast to amyloid plaques in the mCWD-infected brain (note that heparinase treatment ablates the HS labelling). **B.** Levels (left) and composition (right) of HS bound to PrP, as measured by LC-MS. Quantified are N-acetylated (N-Ac), unsubstituted glucosamine (NH₂), N-sulfated (N-S), 2O-sulfated, and

6O-sulfated. Brain regions shown for HS stain in panel (A): ME7: cerebral cortex (WT) and thalamus (*Prnp*^{187N}); mNS: cerebral cortex (WT and *Prnp*^{187N}). Scale bar = 50 μ m.

Author Manuscript

Author Manuscript

Author Manuscript

Author Manuscript

Table 1.

Incubation times for WT or *Prnp*^{187N} mice inoculated with RML, 22L, ME7, or mNS prion strains. Attack rate was 100% for all inoculated mice.

Host	Prion	Passage	Number of mice	Incubation time Mean ± SEM (days)
WT	RML		4/4	144 ± 5
<i>Prnp</i> ^{187N}	RML	1	9/9	252 ± 6
<i>Prnp</i> ^{187N}	<i>Prnp</i> ^{187N} -RML	2	5/5	175 ± 2
<i>Prnp</i> ^{187N}	<i>Prnp</i> ^{187N} -RML	3	5/5	173 ± 5
WT	22L		4/4	140 ± 2
<i>Prnp</i> ^{187N}	22L	1	11/11	173 ± 3
<i>Prnp</i> ^{187N}	<i>Prnp</i> ^{187N} -22L	2	5/5	184 ± 2
<i>Prnp</i> ^{187N}	<i>Prnp</i> ^{187N} -22L	3	5/5	155 ± 9
WT	ME7		4/4	203 ± 25
<i>Prnp</i> ^{187N}	ME7	1	9/9	429 ± 9
<i>Prnp</i> ^{187N}	<i>Prnp</i> ^{187N} -ME7	2	4/4	207 ± 1
<i>Prnp</i> ^{187N}	<i>Prnp</i> ^{187N} -ME7	3	4/4	164 ± 1
WT	mNS		4/4	205 ± 4
<i>Prnp</i> ^{187N}	mNS	1	7/7	428 ± 22
<i>Prnp</i> ^{187N}	<i>Prnp</i> ^{187N} -mNS	2	5/5	205 ± 0
<i>Prnp</i> ^{187N}	<i>Prnp</i> ^{187N} -mNS	3	3/3	200 ± 1